Author/s:
Luo, Z;Neville, SL;Campbell, R;Morey, JR;Menon, S;Thomas, M;Eijkelkamp, BA;Ween, MP;Huston, WM;Kobe, B;McDevitt, CA

Title:
Structure and Metal Binding Properties of Chlamydia trachomatis YtgA

Date:
2020-01

Citation:
Luo, Z., Neville, S. L., Campbell, R., Morey, J. R., Menon, S., Thomas, M., Eijkelkamp, B. A., Ween, M. P., Huston, W. M., Kobe, B. & McDevitt, C. A. (2020). Structure and Metal Binding Properties of Chlamydia trachomatis YtgA. Journal of Bacteriology, 202 (1), https://doi.org/10.1128/JB.00580-19.

Persistent Link:
https://hdl.handle.net/11343/339557

AMERICAN SOCIETY FOR MICROBIOLOGY | Journal of Bacteriology®

RESEARCH ARTICLE

Structure and Metal Binding Properties of *Chlamydia trachomatis* YtgA

Zhenyao Luo,[a,b,c] Stephanie L. Neville,[d,e] Rebecca Campbell,[e] Jacqueline R. Morey,[e] Shruti Menon,[f] Mark Thomas,[g] Bart A. Eijkelkamp,[e] Miranda P. Ween,[e] Wilhelmina M. Huston,[g] Bostjan Kobe,[a,b,c] Christopher A. McDevitt[d,e]

[a]School of Chemistry and Molecular Biosciences, University of Queensland, Brisbane, Queensland, Australia
[b]Australian Infectious Diseases Research Centre, University of Queensland, Brisbane, Queensland, Australia
[c]Institute for Molecular Bioscience, University of Queensland, Brisbane, Queensland, Australia
[d]Department of Microbiology and Immunology, The Peter Doherty Institute for Infection and Immunity, University of Melbourne, Melbourne, Victoria, Australia
[e]School of Biological Sciences, University of Adelaide, Adelaide, South Australia, Australia
[f]School of Biomedical Sciences, Queensland University of Technology, Brisbane, Queensland, Australia
[g]School of Life Sciences, University of Technology Sydney, Ultimo, New South Wales, Australia

ABSTRACT The obligate intracellular pathogen *Chlamydia trachomatis* is a globally significant cause of sexually transmitted bacterial infections and the leading etiological agent of preventable blindness. The first-row transition metal iron (Fe) plays critical roles in chlamydial cell biology, and acquisition of this nutrient is essential for the survival and virulence of the pathogen. Nevertheless, how *C. trachomatis* acquires Fe from host cells is not well understood, since it lacks genes encoding known siderophore biosynthetic pathways, receptors for host Fe storage proteins, and the Fe acquisition machinery common to many bacteria. Recent studies have suggested that *C. trachomatis* directly acquires host Fe via the ATP-binding cassette permease YtgABCD. Here, we characterized YtgA, the periplasmic solute binding protein component of the transport pathway, which has been implicated in scavenging Fe(III) ions. The structure of Fe(III)-bound YtgA was determined at 2.0-Å resolution with the bound ion coordinated via a novel geometry (3 Ns, 2 Os [3N2O]). This unusual coordination suggested a highly plastic metal binding site in YtgA capable of interacting with other cations. Biochemical analyses showed that the metal binding site of YtgA was not restricted to interaction with only Fe(III) ions but could bind all transition metal ions examined. However, only Mn(II), Fe(II), and Ni(II) ions bound reversibly to YtgA, with Fe being the most abundant cellular transition metal in *C. trachomatis*. Collectively, these findings show that YtgA is the metal-recruiting component of the YtgABCD permease and is most likely involved in the acquisition of Fe(II) and Mn(II) from host cells.

IMPORTANCE *Chlamydia trachomatis* is the most common bacterial sexually transmitted infection in developed countries, with an estimated global prevalence of 4.2% in the 15- to 49-year age group. Although infection is asymptomatic in more than 80% of infected women, about 10% of cases result in serious disease. Infection by *C. trachomatis* is dependent on the ability to acquire essential nutrients, such as the transition metal iron, from host cells. In this study, we show that iron is the most abundant transition metal in *C. trachomatis* and report the structural and biochemical properties of the iron-recruiting protein YtgA. Knowledge of the high-resolution structure of YtgA will provide a platform for future structure-based antimicrobial design approaches.

KEYWORDS YtgA, solute binding protein, *Chlamydia trachomatis*, iron acquisition, ABC transporter, heavy metals, iron, structural biology, substrate binding protein

Citation Luo Z, Neville SL, Campbell R, Morey JR, Menon S, Thomas M, Eijkelkamp BA, Ween MP, Huston WM, Kobe B, McDevitt CA. 2020. Structure and metal binding properties of *Chlamydia trachomatis* YtgA. J Bacteriol 202:e00580-19. https://doi.org/10.1128/JB.00580-19.

Editor Ann M. Stock, Rutgers University-Robert Wood Johnson Medical School

Address correspondence to Bostjan Kobe, b.kobe@uq.edu.au, or Christopher A. McDevitt, christopher.mcdevitt@unimelb.edu.au.

Received 11 September 2019
Accepted 8 October 2019
Accepted manuscript posted online 14 October 2019
Published 6 December 2019

Iron (Fe) is an essential micronutrient for nearly all forms of life (1–3). In prokaryotes, Fe is frequently used as a cofactor in redox-dependent processes or in central biochemical pathways, including aerobic respiration, DNA repair, and cellular metabolism (4–6). *Chlamydia trachomatis* is the causative agent of the most prevalent bacterial sexually transmitted infection worldwide and the leading cause of preventable blindness (7, 8). It is estimated that more than 100 million new chlamydial infection cases are diagnosed annually worldwide (9). As an obligate intracellular pathogen, this Gram-negative bacterium invades and grows within eukaryotic cells and scavenges nutrients from the intracellular environment of the host cell (10, 11). Analysis of the *C. trachomatis* genome reveals that despite its small genome of ~1 Mbp, *C. trachomatis* possesses the genes that encode a complete aerobic respiratory chain that includes sodium-motive NADH-quinone oxidoreductase, succinate dehydrogenase, and the cytochrome *bd* complex (12), all of which are Fe-containing proteins. This implies that Fe is required for chlamydial cellular metabolism. In addition, functional studies have provided evidence for an Fe requirement in host cell interaction. Starvation of Fe forces *C. trachomatis* to enter a metabolically active, yet noninfectious reticulate body form (13), with reversion to the infectious form upon relief of Fe-restrictive conditions (14). Collectively, these data indicate that Fe acquisition is essential for *C. trachomatis* survival and pathogenicity.

In biological systems, Fe commonly exists in two oxidative states: ferrous [Fe(II)] or ferric [Fe(III)]. Prokaryotic acquisition of Fe is predominantly facilitated by siderophores and their receptors that capture and internalize Fe(III) from the extracellular environment (15) and/or surface receptors that capture Fe-containing proteins/molecules from the host, such as transferrin, lactoferrin, and heme (16). Some bacteria are also capable of directly acquiring Fe in the ferrous form through transporters such as FeoABC from *Escherichia coli* K-12 (17), and YfeABC from *Yersinia pestis* (18). Genome sequencing has revealed that *C. trachomatis* does not encode protein homologs of known siderophore biosynthetic pathways or surface receptor proteins involved in scavenging host-iron storage proteins/heme, which are common components of Fe acquisition systems in other bacteria. To date, the only putative Fe acquisition system identified in *C. trachomatis* is the ATP-binding cassette (ABC) permease YtgABCD, which is comprised of YtgA, a periplasmic solute binding protein (SBP), a cytoplasmic nucleotide binding domain (YtgB) and a transmembrane channel formed by YtgC and YtgD. Sequence analyses of YtgA indicate that it shares homology with the ABC transporter SBPs involved in the recruitment of metal ions (cluster A-I) and metal chelates (cluster A-II). Prior studies of YtgA have proposed that the protein is specific for Fe(III) (19). However, the amino acid composition of the presumptive metal binding site and the associated bioinorganic chemistry strongly suggest that YtgA may have the capacity to interact with other first row transition metal ions such as Mn(II), but this has remained poorly defined.

Here, we combined X-ray crystallography with differential scanning fluorimetry and metal binding assays to elucidate the structural and metal binding properties of *C. trachomatis* serovar D/UW-3/Cx YtgA. We report the first high-resolution structure of the protein, determined to 2.0-Å resolution in the Fe(III)-bound state. Although YtgA shares a common fold with other members of the cluster A-I subgroup of SBPs, we show that the protein has a highly plastic metal binding site capable of offering a range of coordination geometries. Analyses of the metal binding properties of YtgA revealed that it was highly permissive for interaction with a broad range of transition metal ions, including Mn(II), Fe(II), Co(II), Ni(II), and Zn(II). Nevertheless, functional specificity in the YtgABCD permease most likely arises from only a subset of these metal ions [Fe(II), Mn(II), and Ni(II)] being readily released from YtgA once bound.

RESULTS

YtgA belongs to a subgroup of SBPs with broad ligand specificity. Comparative sequence analysis of *C. trachomatis* YtgA with 31 functionally characterized cluster A-I and A-II SBPs revealed that the protein clustered with a subgroup of cluster A-I SBPs

(a)

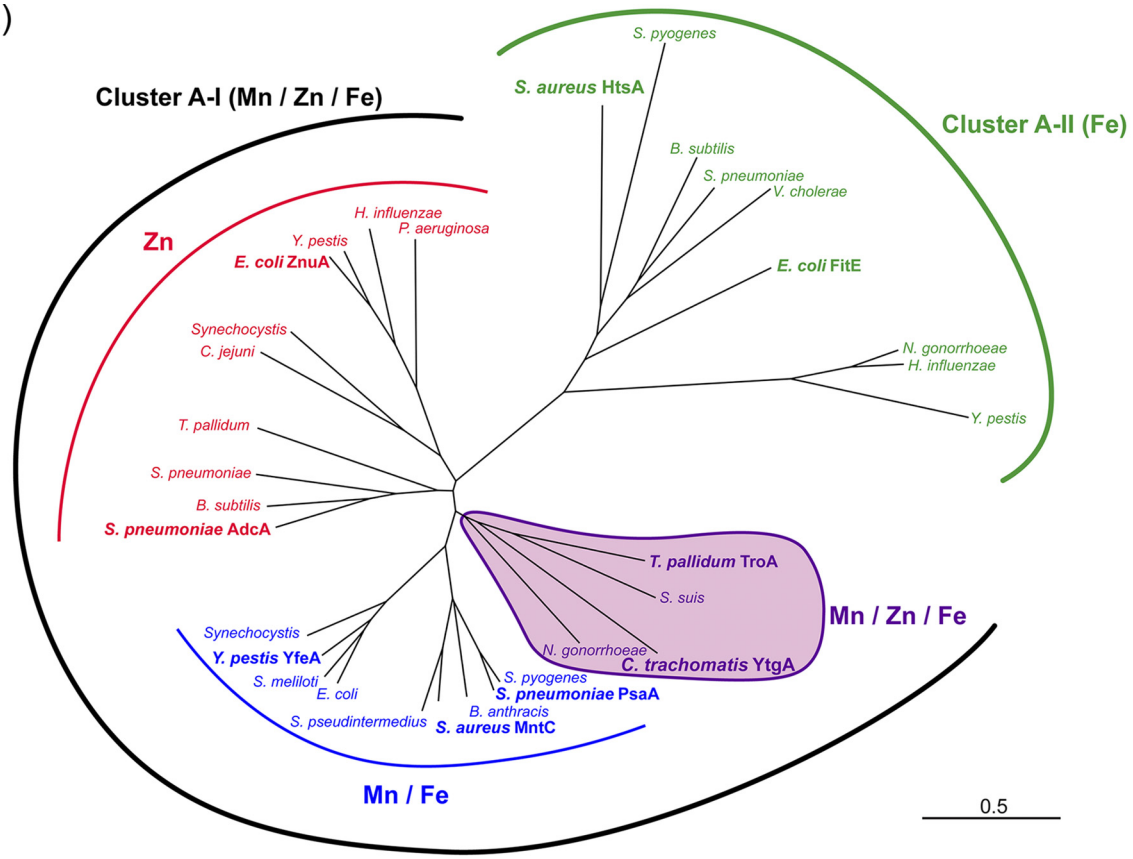

(b)

```
YtgA_Ctr  ASL-RKHLEGNPK------VVDLGQRLLN--------K---NCFDLLSEEGFPDPHIWTD 145
ZnuA_Eco  MQKPVSKLPGAKQVTI-AQLEDVKPLLMKSIHGDDDDHDHAEKSDEDHHHGDFNMHLWLS 147
AdcA_Spn  --TWVPKLLDTLDKKKVKTIKATGDMLLL-PGGEEEEGD--HDHGEEGHHHEFDPHVWLS 144
TroA_Tpa  MGEVFSKLRGSRL------VVAVSE-------TIPV------SQRLSLEEAEFDPHVWFD 137
TroA_Sps  MVEALEKTGV----------AVSK-------NFNA-KD--LNTMDEDGEEIVDPHFWFS 108
MntC_Sau  --RWFEQFLGNVKDVP---SVVLTE-------GIEP-I----PIADGPYTDKPNPHAWMS 158
PsaA_Spn  GNAWFTKLVENAKKTENKDYFAVSD-------GVDV-I----YLEGQNEKGKEDPHAWLN 143
```

FIG 1 Phylogenetic analysis of *C. trachomatis* YtgA. (a) YtgA was aligned to the amino acid sequences of 31 other characterized cluster A-I and A-II SBPs using Clustal Omega. The resulting tree, generated using the neighbor-joining method, displays four main clades comprising the cluster A-II SBPs (green) and the cluster A-I SBPs subgroups associated with zinc binding (red), manganese and/or iron binding (blue), and a clade of SBPs with broad (Mn, Zn and Fe) substrate specificity (shaded purple). *C. trachomatis* YtgA clusters with the latter group. (b) Sequence alignments comparing the region enriched for acidic amino acids in zinc-specific SBPs with *C. trachomatis* YtgA and representative cluster A-I SBPs from the other clades. Amino acid sequences are colored according to the clustering in panel a, with the acidic residue region enriched in zinc-specific SBPs highlighted in yellow and residue numbers shown. The sequences aligned using Clustal Omega were as follows: YtgA_Ctr, *C. trachomatis* YtgA (GI:73811687); ZnuA_Eco, *E. coli* ZnuA (GI:635897169); AdcA_Spn, *S. pneumoniae* AdcA (GI:116516060); TroA_Tpa, *T. palladium* (GI:504108253); TroA_Sps, *S. suis* (GI:386583456); MntC_Sau, *S. aureus* MntC (GI:88194402); and PsaA_Spn, *S. pneumoniae* PsaA (GI:116515973).

that have broad ligand specificity [i.e., interaction with Mn(II), Fe(II), and/or Zn(II)] (Fig. 1a). This subgroup shares sequence identities of ≥20% over the core protein fold (over >200 amino acids) and is distinct from the Fe-recruiting cluster A-II SBPs, which bind metal chelates, and the closely related Zn(II)-specific cluster A-I SBPs. Notably, Zn(II)-specific SBPs frequently possess an acidic amino acid enriched region that is absent from YtgA (Fig. 1b) (20, 21). YtgA orthologs from other chlamydial species, namely, *C. muridarum*, *C. suis*, *C. psittaci*, and *C. pneumoniae*, share sequence identities ranging from 57 to 85% (over >300 amino acids). Notably, the metal binding site residues in YtgA orthologs are strictly conserved (Fig. 2). Taken together, these data suggest that YtgA directly interacts with the ionic form of metals and may not be restricted to binding only Fe(III) ions as previously reported (19).

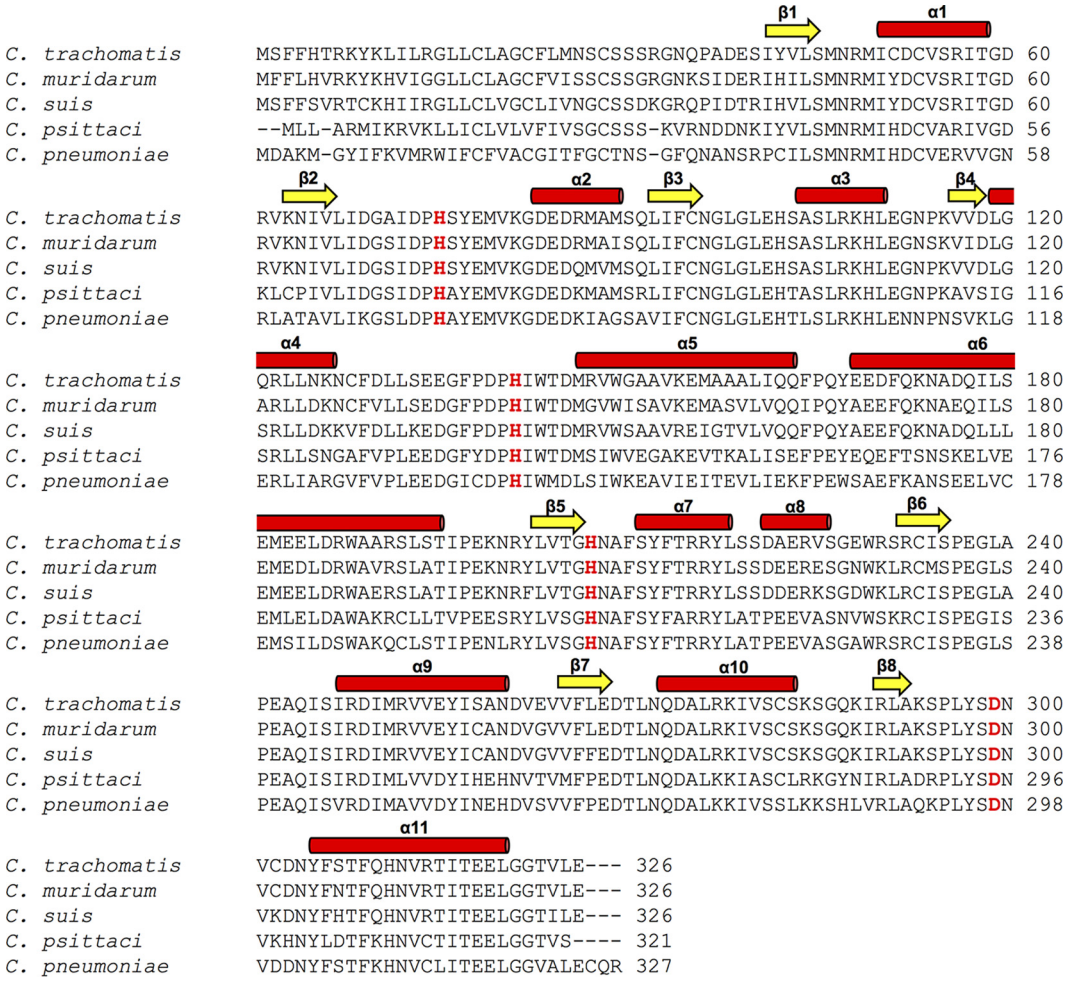

FIG 2 Sequence comparison and secondary structure prediction of chlamydial YtgA proteins. Sequences were aligned using Clustal Omega, using full-length YtgA amino acid sequences from *C. trachomatis* (GI:73811687), *C. muridarum* (GI:497916051), *C. suis* (GI:737424856), *C. psittaci* (GI:493386917), and *C. pneumoniae* (GI:33236198). Metal-coordinating residues are indicated in red. Elements of secondary structure (cylinders, α-helix; arrows, β-strand) were assigned to the sequences based on the crystal structure of *C. trachomatis* YtgA resolved in this study. Numbers of the amino acids are indicated at the end of each line.

YtgA interacts with a broad range of divalent transition metal ions. To investigate the metal binding properties of *C. trachomatis* YtgA, we expressed a recombinant C-terminal dodecahistidine-tagged variant without the putative Sec-type signal peptide (residues 34 to 326) (22). Recombinant YtgA was purified by immobilized metal affinity chromatography, the affinity tag was removed, and the protein was further purified by size exclusion chromatography (SEC) (Fig. 3a). SEC showed that recombinant YtgA was isolated as a single monodisperse species with a relative molecular mass of 36.2 kDa (based on molecular mass standards), which matched closely the predicted molecular mass (36.1 kDa) of recombinant, tag-cleaved monomeric YtgA (Fig. 3b). Endogenous metals, which may have copurified, were removed by denaturation at pH 4.0 in the presence of 20 mM EDTA prior to refolding by dialysis in 20 mM Tris-HCl (pH 7.2)–200 mM NaCl. Inductively coupled plasma-mass spectrometry (ICP-MS) analysis of refolded, tag-cleaved YtgA showed that it was metal free, containing $<$0.01 mol of metal ions per mol of protein.

The interaction of recombinant YtgA with metal ions was first assessed by differential scanning fluorimetry (DSF) using the environmentally sensitive probe SYPRO Orange (23). DSF was performed with a range of physiologically relevant metal ions [Mg(II), Ca(II), Mn(II), Fe(II), Fe(III), Co(II), Ni(II), Cu(II), and Zn(II)] to ascertain which metals

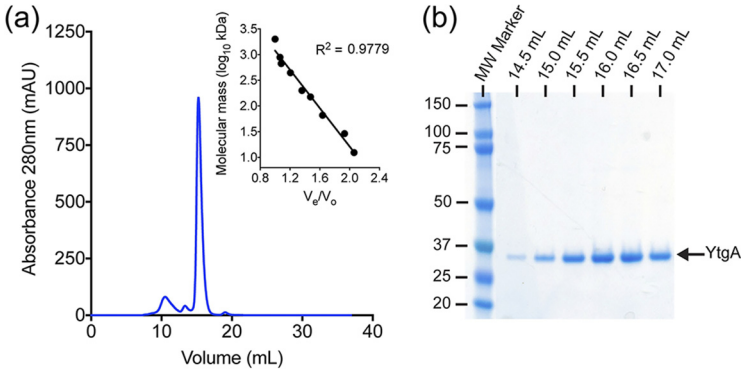

FIG 3 Purification and biochemical characterization of YtgA. (a) Determination of the apparent molecular mass of tag-free YtgA by size exclusion chromatography on a Superdex 200 10/300 column. The inset shows the linear regression of the protein molecular weight standards used to calibrate the column. YtgA eluted with a monomeric molecular mass of 36.2 kDa. (b) Coomassie blue-stained 12.5% SDS polyacrylamide gel showing purified YtgA (arrow).

interacted with the protein. We also examined interaction with Cd(II), since this metal has been shown to bind to a related cluster A-I SBP (23). DSF analyses revealed that metal-free YtgA had a T_m ± the standard deviation (SD) of 50.5 ± 0.9°C (Table 1 and Fig. 4). Treatment with a 10-fold molar excess of Mg(II), Ca(II), or Fe(III) did not significantly alter the T_m of the protein (Table 1 and Fig. 4) ($\Delta T_m \leq 2$°C; $P > 0.05$). Modest, but significant shifts in the T_m of YtgA were observed with Mn(II), Fe(II), and Ni(II) ($P < 0.001$), while larger shifts (>10°C) were observed for Co(II), Zn(II), and Cd(II) ions ($P < 0.001$). Although interaction of Cu(II) with YtgA was tested, the addition of Cu(II) resulted in precipitation of YtgA upon supplementation; thus, data could not be collected. These data show that YtgA is capable of interacting with a broad range of metal ions similar to other members of the Mn/Zn/Fe clade of cluster A-I SBPs. However, these findings also contrast starkly with those reported by Miller et al. (19), who concluded that YtgA was a specific Fe(III)-binding SBP. We speculate that the interaction of Fe(III) with YtgA in that study may be attributable to the higher ratio of metal to protein used. Consequently, we further analyzed YtgA and observed a modest positive shift in the protein T_m (+6.3°C) at higher Fe(III)-protein ratios (≥100-fold molar excess) (Fig. 4h). These data show that Fe(III) can bind to YtgA, although it may have a poor on rate.

YtgA and Fe(II). To complement the DSF analyses, we directly probed the metal binding properties of YtgA by ICP-MS. Here, *in vitro* metal binding assays were conducted using metal-free YtgA and a 10-fold molar excess of the transition metal ions Mn(II), Fe(II), Fe(III), Co(II), Ni(II), Zn(II), and Cd(II). ICP-MS analyses revealed that YtgA

TABLE 1 Effect of divalent cations on the melting temperature of YtgA

Protein[a]	Avg T_m (°C) ± SD[b]	ΔT_m (°C)
Metal-free YtgA	50.52 ± 0.87	
Mg(II)-YtgA	49.65 ± 2.83	–1.0
Ca(II)-YtgA	48.97 ± 3.05	–1.0
Mn(II)-YtgA	58.82 ± 1.51	+7.7[c]
Fe(II)-YtgA	61.94 ± 0.95	+9.8[c]
Fe(III)-YtgA	51.38 ± 0.61	+0.7
Co(II)-YtgA	76.01 ± 1.13	+25.4[c]
Ni(II)-YtgA	63.26 ± 1.55	+12.6[c]
Cu(II)-YtgA	ND[d]	
Zn(II)-YtgA	71.59 ± 1.59	+16.6[c]
Cd(II)-YtgA	71.83 ± 0.59	+19.9[c]

[a]Melting curves for cations that induce a T_m shift are shown in Fig. 4.
[b]Values represent averages and standard deviations from at least three independent measurements.
[c]Statistically significant difference from metal-free protein T_m (one-way ANOVA with Tukey posttest).
[d]ND, not determined.

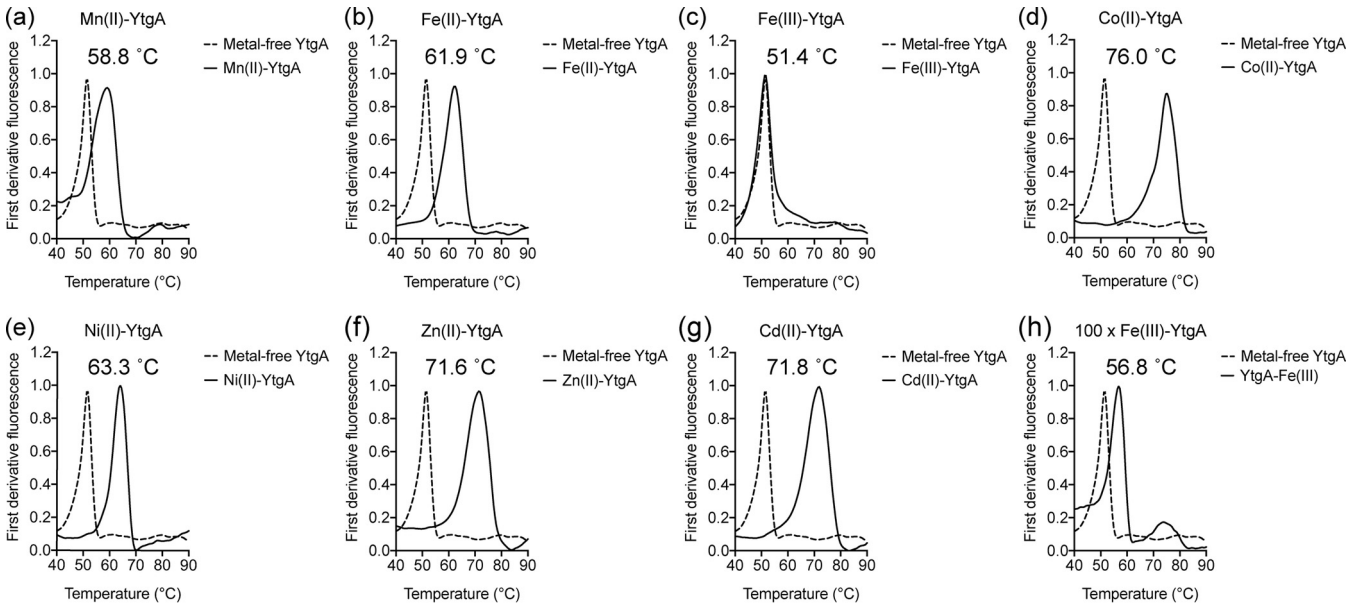

FIG 4 DSF analyses of YtgA. Thermostability of demetallated, tag-free YtgA and metal-incubated YtgA with a 10-fold concentration of the indicated transition metal ion—Mn(II) (a), Fe(II) (b), Fe(III) (c), Co(II) (d), Ni(II) (e), Zn(II) (f), and Cd(II) (g)—or a 100-fold concentration of Fe(III) (h). The data are presented as the first derivative of the SYPRO Orange fluorescence with the inflection point value (T_m) of the solid line shown.

bound all metal ions with stoichiometries of ~1 mol metal ion per mol of protein (Fig. 5). Thus, our data show that the metal binding site of YtgA is capable of binding one metal ion per protein molecule and is not restricted to interaction with only Fe(III) ions. We then assessed the stability of the YtgA-metal complexes by treatment with a 100-fold molar excess of the strong chelating agent EDTA, which has affinities for transition metal ions in the range of $\sim 10^{-13}$ to 10^{-25} M (24). The affinities of cluster A-I SBPs for metal ions are several orders of magnitude less and are typically in the range of $\sim 10^{-7}$ to 10^{-9} M (20, 25). Here, we observed that the metal ions Mn(II), Fe(II), and Ni(II) were efficaciously removed by EDTA (Fig. 5). This result contrasts starkly with Fe(III), Co(II), Zn(II), and Cd(II), which formed YtgA-metal complexes that were essentially irreversible (extraction $\leq$ 15%) (Fig. 5). These ions were only extracted from YtgA by unfolding the protein in the presence of EDTA. It is a physiological requirement for transport that the bound metal ion can be readily released from the SBP to the transporter. Taken together, our data suggest that Mn(II), Fe(II), and Ni(II) are potential physiological ligands of YtgA. In contrast, although Fe(III), Co(II), and Zn(II) can bind to

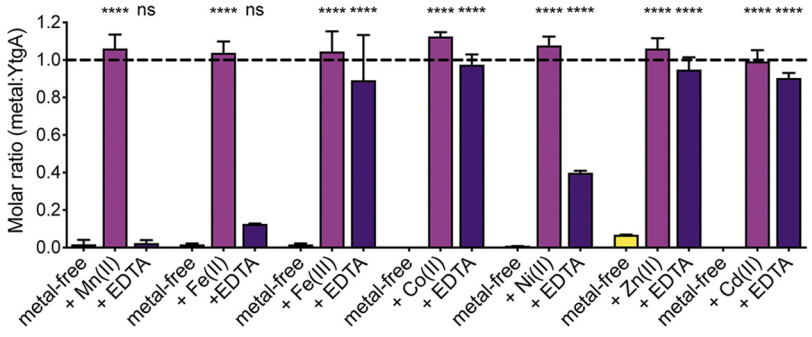

FIG 5 Transition metal-ion interaction with YtgA. *In vitro* metal-binding experiments with demetallated, tag-free YtgA and transition metal ions as shown and analyzed by ICP-MS. The molar ratio of metal ion to YtgA was determined, and data correspond to mean values ± the SD from at least four independent biological experiments. Statistical significance of the differences relative to demetallated, tag-free YtgA was determined by one-way ANOVA with the Sidak posttest (ns, not significant; ****, $P < 0.0001$).

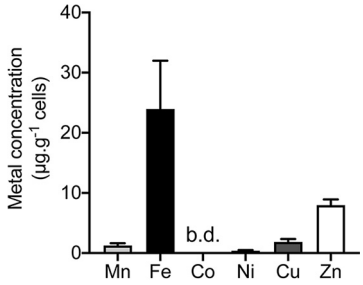

FIG 6 Cellular metal accumulation of *C. trachomatis*. Total cellular metal-ion accumulation of *C. trachomatis* elementary bodies represented as the concentration (means ± the SD) of ions per cell, determined as μg of metal g^{-1} cells (dry weight). The values are from two independent biological experiments. The metal ions assessed were Mn, Fe, Co, Ni, Cu, and Zn. b.d., below detection.

YtgA, the stabilities of the resultant protein-metal complexes are unlikely to permit release of the ions to the YtgBCD transporter for cytoplasmic import.

To better understand the physiological context of YtgA and metal transport, we performed whole-cell ICP-MS on *C. trachomatis* infectious elementary bodies. This revealed that Fe was the most abundant transition metal ion (Fig. 6), with the other metals having lower abundance, which can be summarized as follows: Fe > Zn > Cu > Mn > Ni. Building on this observation, we further explored the potential role of YtgA in *C. trachomatis* Fe(II) acquisition.

Structural analyses of YtgA. To further our understanding of *C. trachomatis* YtgA, a high-resolution structure of the protein was determined by X-ray crystallography. Although crystallization of the protein with Fe(II), the presumptive physiological ligand, was attempted, oxidation to Fe(III) occurred during the crystallization process, based on the observed solution color. The YtgA crystal diffracted to 2.0-Å resolution. One molecule of YtgA was present in each asymmetrical unit. Residues 34 to 39 and residues 285 to 286 were not modeled in the refined structure due to a lack of electron density in the corresponding regions. The crystallographic refinement statistics are summarized in Table 2.

YtgA comprises two globular domains, denoted as N- and C-terminal domains, and a domain-linking helix (α6) that spans the entire molecule (Fig. 7a and b). Similar to other cluster A-I SBPs, the interdomain helix would most likely preclude large conformational motion of either domain, as reported for *S. pneumoniae* PsaA (26) and *Yersinia pestis* YfeA (27, 28) (Fig. 8). This is in stark contrast to the shorter, flexible interdomain linkages present in non-metal-binding SBPs, such as the amino acid-binding SBP LivJ (29, 30), that permit larger movement (up to 60°) of the two domains. In YtgA, the N- and C-terminal domains both comprise five α-helices (N-terminal: α1, α2, α3, α4, and α5; C-terminal: α7, α8, α9, α10, and α11) that each flank a four-stranded β-sheet (N-terminal: β1, β2, β3, and β4; C-terminal: β5, β6, β7, and β8) at the center (Fig. 7a and b). The metal binding site resides at the interface between the two domains and is located ~10 Å beneath the molecular surface of the protein. One Fe(III) ion, with full occupancy, is present at the metal binding site of the protein, with the two globular domains closed over this region. In related cluster A-I SBPs, such as *Streptococcus pneumoniae* PsaA, this conformation represents the closed, ligand-bound form of the protein and is distinct from the open, metal-free state (31). In YtgA, the loop connecting α9 and β6 on the surface of the C-terminal domain dwells directly above the bound Fe(III) ion. Together, these features bury the metal ion and the binding-site, shielding them from the bulk solvent in the closed, metal-bound state (Fig. 7c). In the binding site, the bound Fe(III) ion forms coordination interactions with the Nε2 atoms from His75, His141, and His207, and the Oδ1 and Oδ2 atoms from Asp299, with the coordination bond lengths of 2.04, 2.14, 2.21, 2.01, and 2.38 Å, respectively, thus giving a distorted three-N, two-O (3N2O) trigonal bipyramidal coordination geometry to the bound metal ion (Fig. 7d).

TABLE 2 Crystallographic data collection and refinement statistics

Parameter[a]	Value[d]
Data collection statistics	
Wavelength (Å)	0.954
Resolution range (Å)	19.08−2.00 (2.07–2.00)
Space group	*C* 1 2 1
Unit cell dimensions	
a, *b*, *c* (Å)	47.8, 61.1, 105.5
α, β, γ (°)	90.0, 96.9, 90.0
Completeness (%)	100.0 (99.9)
R_{merge}[a]	0.09 (1.00)
R_{pim}[b]	0.04 (0.39)
CC(1/2)	0.99 (0.69)
$<I/\sigma(I)>$	16.51 (2.03)
Multiplicity	7.3 (7.2)
No. of unique reflections	20,476 (2,001)
Refinement statistics	
R_{work}/R_{free} (%)[c]	17.9/22.5
No. of atoms	
Protein	2,324
Ligand/ion	4
Water	208
Avg B factor (Å^2)	
Protein	38.9
Ligand/ion	40.8
Water	42.1
RMSD	
Bond length (Å)	0.01
Bond angle (°)	0.89

[a] $R_{merge} = \sum_{hkl}\sum_j|I_{hkl,j} - \langle I_{hkl}\rangle|/(\sum_{hkl}\sum_j I_{hkl,j})$.
[b] $R_{pim} = \sum_{hkl}\sqrt{n/(n-1)}\sum_j|I_{hkl,j} - \langle I_{hkl}\rangle|/(\sum_{hkl}\sum_j I_{hkl,j})$.
[c] $R_{work}/R_{free} = \sum_{hkl}|F^{obs}_{hkl} - F^{calc}_{hkl}|/(\sum_{hkl}F^{obs}_{hkl})$. R_{free} was calculated using a randomly chosen 5% fraction of data that was excluded from refinement.
[d] Values in parentheses correspond to the highest-resolution shell.

Overall, YtgA possesses a structural fold highly conserved among cluster A-I SBPs, including *Treponema pallidum* Zn(II)-binding SBP TroA (32) (PDB 1TOA), *Streptococcus pyogenes* Fe(II/III) SBP MtsA (33) (PDB 3HH8), *Yersinia pestis* Fe/Mn(II) SBP YfeA (27) (PDB 5UY4), *Staphylococcus aureus* Mn(II)-binding SBP MntC (34) (PDB 4K3V), *Staphylococcus pseudintermedius* Mn(II) SBP SitA (35) (PDB 4OXR), and *S. pneumoniae* Mn(II)-binding SBP PsaA (36) (PDB 3ZTT). Superimposing the crystal structures backbones revealed low root mean square deviation (RMSD) values (<1.1 Å) between YtgA and the other SBP structures (Fig. 9a and b; Table 3), despite the low level of overall sequence identity (<26%) between them. Notably, three of the four metal-coordinating ligands in YtgA, namely, His75, His141, and Asp299, are strictly conserved through all cluster A-I SBPs compared in this study. Interestingly, the fourth metal-coordinating position in YtgA presents a histidine residue (His207), which resembles Zn(II)-specific SBPs, such as ZnuA and AdcAII, and TroA, which has been implicated as having a physiological role in Zn(II) acquisition (Fig. 9c). In contrast, structurally characterized SBPs that favor interaction with Fe, such as MtsA and YfeA (Fig. 9d), or with Mn(II), such PsaA and MntC (Fig. 9e), present an acidic residue at this location. Another distinct structural feature of YtgA is that the protein possesses five helices in each of its globular domains, as opposed to the four-helices-per-domain arrangement observed in other cluster A-I SBPs (Fig. 9b). The extra helices (α4 in the N-terminal domain and α8 in the C-terminal domain) are positioned on the same side of the molecule, relative to the domain-linking helix (Fig. 9a and b). Whether these extra structural elements play a role in cargo acquisition or recognition by YtgBCD permease remains to be determined.

S. pyogenes MtsA and *Yersinia pestis* YfeA are among the cluster A-I SBPs that show binding preference for Fe(III) (27, 33). Comparing the metal-bound states of YtgA and MtsA shows that although a single Fe(III) ion is present in both structures and adopts

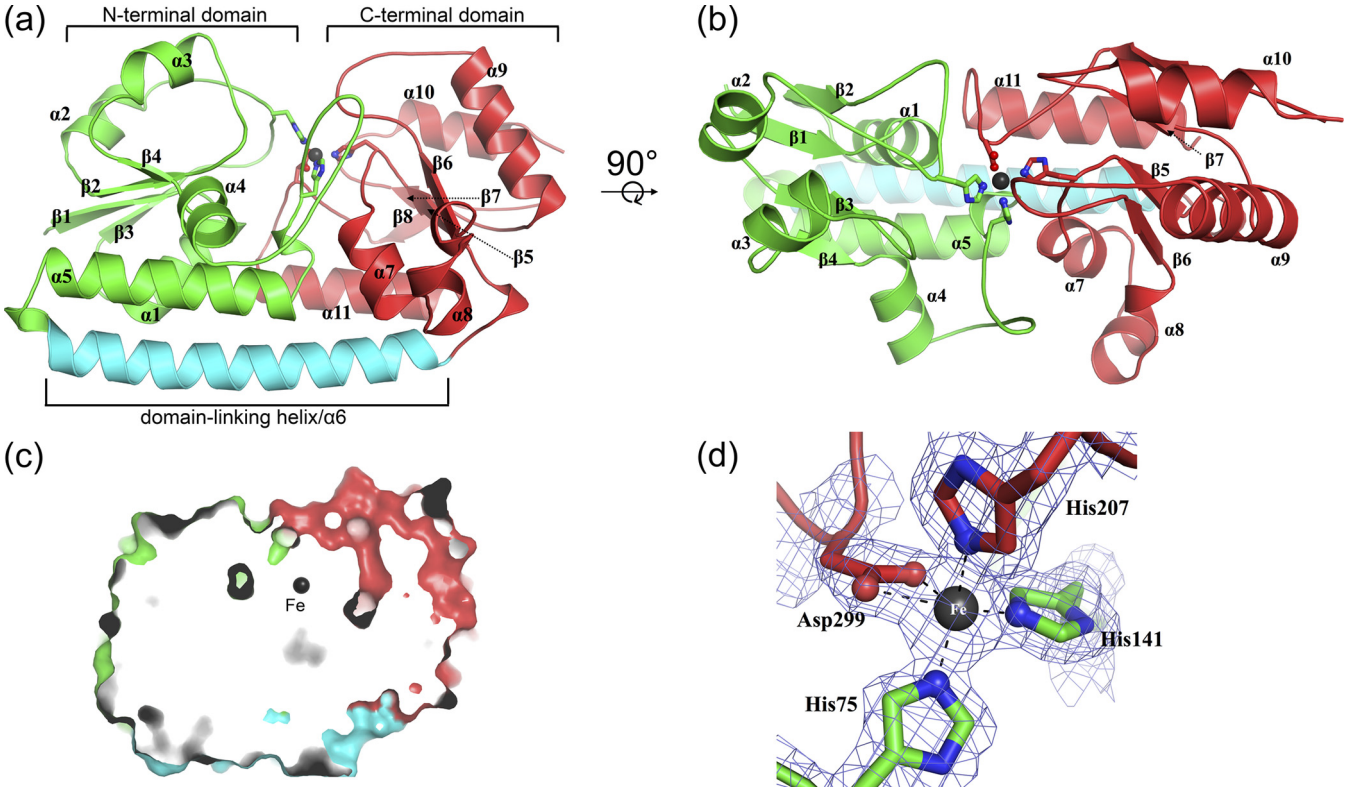

FIG 7 Crystal structure of Fe(III)-bound YtgA. (a and b) "Side" (a) and "top" (b) views of a cartoon illustration of Fe-bound, tag-free YtgA in the closed conformation. The protein consists of N-terminal (green) and C-terminal (red) globular domains with a domain-linking helix (cyan). All the secondary structures are labeled with black text. The metal-binding site situates at the interface between the two domains. The bound Fe atom is shown by a black sphere and its coordinating residues are in stick representation. (c) Surface "side" view of YtgA crystal structure. The bound Fe (black sphere) is completely buried in the protein. The N-terminal domain, C-terminal domain, and domain-linking helix are shown in green, red, and cyan, respectively. (d) Metal binding site of YtgA. The bound Fe (black sphere) is coordinated by three nitrogen atoms from His75, His141, and His207, respectively, and two oxygen atoms from Asp299 in a distorted trigonal bipyramidal geometry. The metal-coordinating residues are shown as a stick-and-ball representation, and the coordination bonds are represented by dashed lines. The $2F_o$-F_c electron density map (blue mesh) shown is contoured at 1.5σ.

a distorted trigonal bipyramidal coordination geometry, the coordinating ligands offered by the metal binding sites are distinctly different. In YtgA, the Fe(III) ion is coordinated by three N and two O atoms. In contrast, in MtsA, the bound Fe(III) ion is coordinated by two N and three O atoms. In YfeA, both of the acidic residues in the metal-binding site contribute to bidentate coordination with Fe(III), resulting in a 2N4O trigonal prism geometry. Notably, the coordination environment present at the YtgA metal-binding site closely resembles that of the Zn(II)-binding SBPs and TroA (32, 37, 38). Although the coordination environments are similar, the acidic residue employs both oxygen atoms to bind Fe(III) in YtgA. This is in contrast to Zn(II)-specific SBPs, where only one oxygen atom from the carboxyl group on the acidic residue is involved in reversible Zn(II) ion coordination.

DISCUSSION

Acquisition of Fe is essential for the survival and virulence of the obligate intracellular pathogen *C. trachomatis*. The scavenging of Fe and other crucial transition metal ions from the extracytoplasmic environment is most commonly facilitated in prokaryotes by cluster A-I SBPs. Iron uptake by *C. trachomatis* is associated with the YtgABCD permease, which has been shown to be regulated by Fe via the DtxR family regulator YtgR (39). Import of Fe was inferred to be facilitated by YtgA due to its previously reported interaction with Fe(III) (19). In this study, we have determined the first high-resolution structure of YtgA and, by combining *in vitro* metal binding and DSF assays, shown that YtgA is a highly promiscuous SBP capable of interaction with a broad range of transition metal ions. These findings challenge earlier conclusions

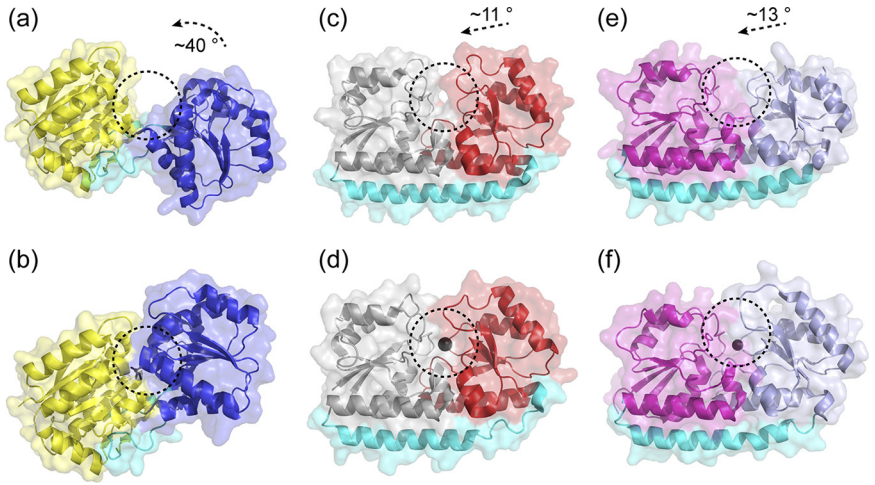

FIG 8 Solute-binding protein conformational movement. (a, c, and e) Surface views of the open, unliganded conformations of LivJ (PDB 1Z15) (a), PsaA (PDB 3ZK7) (c), and YfeA (PDB 6Q1C) (e). (b, d, and f) Surface views of the closed, ligand-bound conformations of LivJ (PDB 1Z16) (b), PsaA (PDB 3ZTT) (d), and YfeA (PDB 5UYG) (f). The N- and C-terminal lobes of each SBP are indicated in yellow and dark blue (LivJ), gray and red (PsaA), and magenta and light blue (YfeA). The domain linking regions are indicated in cyan in all structures. The bound solute molecule in each structure is represented by a black stick or spheres. The binding sites in each SBP are highlighted with a dashed circle. The relative movement of the C-terminal lobe onto the N-terminal lobe of each SBP is indicated by arrows.

regarding the physiological ligand(s) of YtgA and the inferred specificity of the YtgABCD permease.

The selective import of metals ions by ABC permeases can largely be ascribed to the specificity of the cluster A-I SBP component. Specificity within these proteins arises

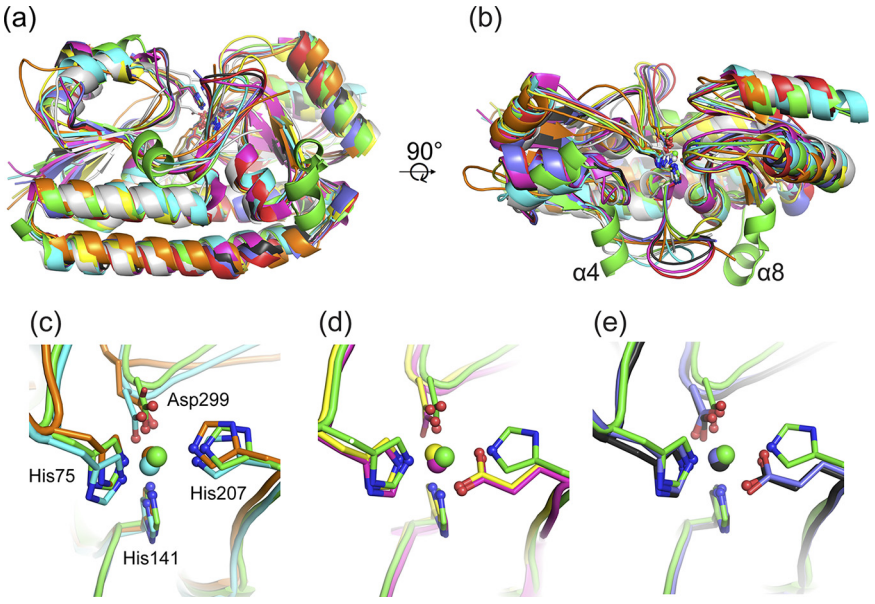

FIG 9 Structural comparison of YtgA with structural homologs. (a and b) "Side" (a) and "top" (b) views of structural superimpositions of selected crystal structures. Colors: green, *C. trachomatis* YtgA; cyan, *T. pallidum* TroA (PDB 1TOA); orange, *S. pneumoniae* AdcAII (PDB 3CX3); magenta, *S. pyogenes* MtsA (PDB 3HH8); yellow, *Y. pestis* YfeA (PDB 5UY4); light blue, *S. aureus* MntC (PDB 4K3V); black, *S. pneumoniae* PsaA (PDB 3ZTT). Bound metal ions are indicated by spheres, and their coordinating residues are shown in stick representation. The unique α-helices of YtgA are labeled. The structures were superimposed using the Cα atoms in PyMOL with comparisons of the metal-binding sites to YtgA shown for Zn(II)-binding SBPs (c), Fe-binding SBPs, (d) and Mn(II)-binding SBPs (e). The metal-coordinating residues are labeled based on YtgA in panel c. Orientations of the view in panels d and e are consistent with the view in panel c. Bound metal ions (spheres) and their coordinating atoms (small spheres) from the respective residues (sticks) are shown.

TABLE 3 Sequence and structural similarities of YtgA with homologous SBPs

Protein	RMSD (Å)	Sequence identity (%)	No. of C_α aligned	PDB ID
T. pallidium TroA	1.00	24.2	261	1TOA
S. pyogenes MtsA	1.15	22.6	255	3HH8
Y. pestis YfeA	1.06	21.9	250	5UY4
S. pseudintermedius SitA	1.34	18.7	264	4OXR
S. pneumoniae PsaA	1.29	22.8	256	3ZTT
E. coli ZnuA	1.85	14.7	179	2PS0
S. aureus MntC	1.07	19.6	226	4K3V
S. pneumoniae AdcAII	1.65	18.8	239	3CX3

from the coordinating environments offered by the metal-binding sites. First-row transition metals utilize their 3d electron orbitals to form coordination bonds with ions that carry lone pair electrons, such as sulfur, oxygen, and nitrogen. The resultant complexes adopt specific spatial geometries due to the directionality of the metal ion 3d-orbitals. Analysis of the available Zn(II)-specific SBP crystal structures reveals that Zn(II) is most frequently associated with tetrahedral (four ligands) complexes, owing to the small ionic radius of the ion. Further, as a soft Lewis acid, Zn(II) tends to interact with soft Lewis bases (40, 41), such as nitrogens in histidines. Mn(II) and Fe(II), which in contrast have larger ionic radii, can accommodate additional ligands with less repulsion energy penalty. Coordination numbers for these metal ions are frequently 5 and 6, with trigonal bipyramidal and octahedral geometries. Mn(II) and Fe(II) are hard Lewis acids that preferentially interact with hard Lewis bases (40, 41), such as the oxygen atoms from water or carboxylate containing amino acids. The high-resolution structure of YtgA shows that the metal binding site is defined by three histidine residues (His75, His141, and His207) and one aspartic acid residue (Asp299), resembling the binding sites frequently found in Zn(II)-specific SBPs such as *Salmonella* ZnuA (42). However, in YtgA, the conformation of Asp299 is not restricted as it is in other cluster A-I SBPs. Consequently, it allows one or both of the oxygen atoms in its carboxylate group to contribute to metal coordination. This arrangement would permit YtgA to provide tetrahedral (3N1O, with three nitrogen atoms from His75, His141, and His207 and one oxygen atom from the monodentate interaction of Asp299), trigonal bipyramidal (3N2O, with three nitrogen atoms from His75, His141, and His207 and two oxygen atoms from the bidentate interaction of Asp299), or octahedral (3N3O, with three nitrogen atoms from His75, His141, and His207, two oxygen atoms from the bidentate interaction of Asp299, and one oxygen atom from a water molecule) metal ion coordination. The balance between the "hardness" and "softness" of the ligands can be fine-tuned by including or excluding extra coordinating oxygen atoms depending on the preference of the interacting metal ion. However, this flexible coordination geometry precludes the capacity for strict selection of only a single metal ion ligand.

The flexibility of YtgA Asp299 has similarity to Asp280 of *Streptococcus pneumoniae* PsaA (31). In PsaA, this equivalent carboxylate residue influences metal ion selection and reversibility of the metal-PsaA complex, resulting in impacts upon metal ion transport (23, 31, 36, 43). Consistent with these insights, YtgA was also shown to be highly promiscuous for interaction with a range of metal ions, despite their preference for distinct coordination geometries. Nevertheless, our analyses also revealed differences in the stabilities of the resultant YtgA-metal complexes. The metal ligands Co(II), Zn(II), and Cd(II) all form highly stable complexes with YtgA, as shown by the large T_m shifts and the inability of EDTA to extract the bound metal ion. Notably, we also observed that YtgA bound Fe(III) irreversibly, rendering Fe(III) an unlikely physiological ligand. This is consistent with the previous finding that YtgA bound Fe(III) could not be replaced by ^{59}Fe(III) (19). Interestingly, the metal ion did not significantly shift the protein T_m at concentrations similar to those of the other metal ligands. We speculate that this may be due to a slow on rate; alternatively, it may reflect a solubility issue associated with the $FeCl_3$ salt in the DSF assay. Irrespective of the precise technical basis for this issue, our data indicate that YtgA stabilization with Fe(III), Co(II), Zn(II), and Cd(II) is highly thermodynamically favorable.

Successful cellular import of transition metal ions is dependent not only on their efficient binding by the SBP but also on subsequent release upon interaction with the ABC transporter. Prior studies of related cluster A-I SBPs have shown that kinetically trapped protein-metal complexes are incapable of releasing the bound metal ions to the transporter (31, 36, 43). Therefore, we propose that Fe(III), Co(II), Zn(II), and Cd(II) are not transported ligands of the YtgABCD permease. Further, these ions could potentially abrogate permease function through the formation of irreversible metal-YtgA complexes. In contrast, Mn(II), Fe(II), and/or Ni(II) are potential physiological ligands with Fe(II), the most likely ligand, given the 19-fold-greater abundance of Fe(II) over Mn(II) in *C. trachomatis* cells. The cytosolic concentrations of these metal ions within the eukaryotic host cell provide additional context for speculation (44). In the cytosol, the labile pools of Fe(II) (0.1 to 1 μM) and Mn(II) (1 μM [45]) are estimated to be at least 4 orders of magnitude greater than those of Zn(II) (50 pM [46]), Co(II), Ni(II), and Cu(II) ions. Although the relative abundance of metal ions within the membrane-bound compartment occupied by *C. trachomatis* in the eukaryotic cell remains unknown, it likely reflects the cytoplasmic abundance. Thus, we infer that the lower abundance of the labile forms of competing metal ions would minimize their potential interactions with YtgA *in vivo*. The balance of evidence indicates that YtgA is most likely involved in Fe(II) uptake, but we cannot exclude the possibility that it also facilitates low-level Mn(II) uptake as well. Current literature suggests that chlamydiae may be able to acquire Fe(II) via the slow-recycling pathway of endocytosed transferrin receptor (3, 47, 48). This system is assumed to rely on the reduction of transferrin-bound Fe(III) to Fe(II) via the host ferrireductase $STEAP_3$ (49) or possibly riboflavin (50), followed by endosome fusion with the chlamydial inclusion (47, 51, 52). Further, it has been suggested that the chlamydial inclusion may interact with both mitochondria and autophagosomes to facilitate the acquisition of essential nutrients (53, 54). Collectively, these mechanisms would allow *C. trachomatis* to scavenge Fe(II) from the host cytosol into the chlamydial inclusion environment, where it could be selectively transported by YtgABCD. Although *C. trachomatis* has an essential requirement for iron, it likely encounters conditions of limited Fe(II) abundance. Bacterial adaptation to iron limitation has been reported to involve numerous cellular responses, one of which is the substitution of Mn(II) for Fe(II) in certain metalloproteins, including class I ribonucleotide reductases (55, 56) and superoxide dismutase (57, 58). Metal ion substitution has been proposed as a mechanism to conserve Fe(II) by restricting its utilization to a subset of metalloproteins during growth under limiting conditions. Therefore, Mn(II) acquisition by YtgA could serve to increase the cellular pool of Mn(II) ions as the cellular abundance of Fe(II) was depleted and thereby enable metal ion substitution. Although not all Fe(II) cofactors are permissive for Mn(II) substitution, this process has been shown to be beneficial in other bacteria during exposure to Fe(II)-restricted conditions. This model may also provide a plausible mechanistic basis for the prior observation that YtgR, the DtxR family metalloregulator that controls expression of the *ytgABCD* operon, can be regulated by Mn(II) ions (19, 59, 60).

Given the high degree of sequence identities among YtgA orthologs, our observations suggest that chlamydial SBPs employ a common metal binding mechanism. Since chlamydiae have a strict iron dependency, the promiscuity of YtgA may arise from the composition of the metal binding site and the associated bioinorganic limitations in achieving selectivity for Fe(II), thereby rendering it permissive for interaction with other ions. Alternatively, it may be that the chemical environment of the chlamydial inclusion excludes these potential competing ions, such that there is no selective pressure for greater selectivity. Further studies on chlamydial inclusions and the structure-function relationships of the metal binding sites in YtgA orthologs will resolve these questions.

Collectively, our work demonstrates that *C. trachomatis* YtgA is a cluster A-I SBP with a new variation in the modality of metal ion coordination (3N2O), as shown for Fe. Although YtgA has been previously reported to be a Fe(III)-specific binding protein, our findings show that YtgA interacts with a range of transition metal ions *in vitro*. Analysis of the stability of protein-metal complexes and whole-cell metal accumulation reveals

that YtgA is most likely involved in the acquisition of Fe(II) but may also recruit Mn(II) from eukaryotic cells. These findings provide new molecular insights into how *C. trachomatis* acquires Fe from host cells and provide a robust foundation for the development of antimicrobials targeting this crucial import pathway.

MATERIALS AND METHODS

Expression and purification of YtgA. Recombinant YtgA was generated by gene synthesis of *C. trachomatis ytgA* serovar D/UW-3/Cx (GenScript), PCR amplification and ligation-independent cloning using the primers YtgA1F (5′-TGGGTGGTGGATTTCCTAACCAGCCGGCAGAT) and Ytg1R (5′-TTGGAAGTAT AAATTTCCTTCCAGGACCGTGCC) to insert the gene into a C-terminal dodecahistidine tag-containing vector, pCAMcLIC01, and generate pCAMcLIC01-YtgA. Protein expression was performed in *Escherichia coli* Lemo21(DE3) by growing the cells in an autoinducing TB medium (Overnight Express; Merck) using UltraYield Flasks (Thomson Instrument Company) for 18 h at 27°C on an Innova 44R shaking incubator at 215 rpm. The cells were harvested, resuspended in 20 mM 4-morpholinepropanesulfonic acid (MOPS; pH 7.2), 200 mM NaCl, 15 mM imidazole, and 20% glycerol buffer, and then disrupted at 30,000 lb/in^2 by a Constant Systems cell disruptor. The soluble supernatant was then isolated by centrifugation at 4°C for 60 min at 120,000 × *g*. Purification of YtgA was achieved by a HisTrap HP column (GE Healthcare, UK) on an ÄKTA purifier (GE Healthcare) using a binding buffer containing 20 mM MOPS (pH 7.8), 200 mM NaCl, 10% glycerol, and 15 mM imidazole, and an elution buffer containing 20 mM MOPS (pH 6.6), 200 mM NaCl, 10% glycerol, and 1 M imidazole. The imidazole was removed by buffer exchange on a HiPrep 26/10 desalting column (GE Healthcare), and sample homogeneity was confirmed by size exclusion chromatography on a Superdex 200 10/30 column (GE Healthcare) using an ÄKTA purifier (GE Healthcare) prior to characterization. Thyroglobulin (669 kDa), apoferritin (443 kDa), β-amylase (200 kDa), alcohol dehydrogenase (150 kDa), albumin (66 kDa), and carbonic anhydrase (29 kDa) were used as molecular weight standards on the Superdex 200 10/30 column, with a blue dextran standard (2 MDa) used to determine the void volume (Sigma-Aldrich).

Metal-free YtgA generation and metal content analysis. Recombinant YtgA had the dodecahistidine tag removed by a 1-h enzymatic digestion at a ratio of 1:25 by the histidine-tagged 3C human rhinovirus protease at a cleavage site introduced between YtgA and the tag. The protein was then reverse purified on a HisTrap HP column (GE Healthcare), with the cleaved protein unable to bind to the column. Removal of the dodecahistidine tag was confirmed by the observed reduction in molecular mass on a 4 to 12% SDS-PAGE gel and confirmed by immunoblotting. Demetallated (metal-free), tag-free YtgA was prepared by dialyzing the protein (10 ml) in a 10-kDa molecular weight cutoff (MWCO) membrane (Pierce) against 4 liters of 20 mM sodium acetate buffer (pH 4.0), with 20 mM EDTA, at 25°C for 24 h. The sample was then dialyzed against 4 liters of 20 mM Tris-HCl (pH 7.2)–200 mM NaCl, at 4°C for 24 h. The sample was then recovered and centrifuged at 120,000 × *g* for 10 min to remove any insoluble material. Demetallated, tag-free YtgA was then desalted into 20 mM MOPS (pH 7.2)–200 mM NaCl, 10% glycerol on a HiPrep 26/10 desalting column (GE Healthcare). Metal content analysis was performed by ICP-MS. Three micromolar protein was heated at 95°C for 15 min in 3.5% HNO_3. The insoluble material was removed by centrifugation at 18,000 × *g* for 20 min, and then the samples were analyzed on an Agilent 7500cx ICP-MS/MS apparatus (Adelaide Microscopy, University of Adelaide).

YtgA metal binding assays. Metal loading assays were performed on demetallated, tag-cleaved YtgA (20 μM) by mixing the samples with a >10-fold molar excess (200 μM) of $MnSO_4$, $FeSO_4$, $FeCl_3$, $CoCl_2$, $NiCl_2$, $CuSO_4$, $ZnSO_4$, and $CdCl_2$ in a total volume of 2 ml into the binding assay buffer (20 mM MOPS [pH 7.2], 200 mM NaCl, 10% glycerol) for 2 h at 4°C. Metal ion stock solutions for the assays were prepared immediately prior to incubation with YtgA to minimize precipitation and, in the case of $FeSO_4$, oxidation of Fe(II) to Fe(III). After incubation, unbound metal was removed by buffer exchange on a PD10 column (GE Healthcare) into the binding assay buffer and the protein concentration was determined. Solutions of metal-loaded protein (1.4 to 2 μM) were prepared in 3.5% HNO_3 and boiled for 15 min at 95°C. Samples were then cooled and centrifuged for 20 min at 18,000 × *g*. The supernatant was then analyzed by ICP-MS, and the protein-to-metal ratio was determined.

Differential scanning fluorimetry. The differential scanning fluorimetry assays were performed essentially as described previously (36). Briefly, 10 μM demetallated, tag-cleaved YtgA in 20 mM MOPS (pH 7.2), 200 mM NaCl, 10% glycerol, and 5× SYPRO Orange (Life Technologies) was incubated in the presence of 100 μM metal ion and then analyzed on a Roche LC480 real-time cycler (Roche Applied Sciences). The samples were preincubated for 10 min with the indicated metal ion concentration and then subjected to thermal unfolding from 37 to 97°C at a heating rate of 1°C per min. Fluorescence data were also collected for buffer only, protein without metal ions, and for each of the metal ions without protein. The fluorescence data were collected by excitation at 470 nm and emission at 570 nm. After subtraction of the background fluorescence from the buffer, the first derivative of the fluorescence data was determined and analyzed using GraphPad Prism to determine the inflection point of the melting transition (T_m). Data from at least three independent experiments were used to determine the mean T_m values ± the SD of wild-type YtgA. The statistical significance of the differences in the T_m shifts was determined by a one-way analysis of variance (ANOVA) using a Tukey posttest.

Phylogeny. The sequences of the 32 SBPs included in this study were obtained from the NCBI under the following GI accession numbers: *Bacillus anthracis* MntA, GI:229264967 (61); *Bacillus subtilis* YcdH, GI:2415736 (62); *Bacillus subtilis* YclQ, GI:758317765 (63); *Campylobacter jejuni* ZnuA, GI:384442496 (64); *Chlamydia trachomatis* YtgA, GI:73811687 (65); *Escherichia coli* FitE, GI:190907145 (66); *Escherichia coli* SitA, GI:84060846 (67); *Escherichia coli* ZnuA, GI:298380994 (68); *Haemophilus influenzae* FbpA, GI:1098687

(69); *Haemophilus influenzae* ZnuA, GI:16272089 (70); *Neisseria gonorrhoeae* FbpA GI:1098687 (71); *Neisseria gonorrhoeae* MntC, GI:59800624 (72); *Pseudomonas aeruginosa* ZnuA, GI:15600691 (20); *Sinorhizobium meliloti* SitA, GI:336034510 (73); *Staphylococcus aureus* HtsA, GI:537378541 (74); *Staphylococcus aureus* MntC, GI:88194402 (75); *Staphylococcus pseudintermedius* SitA, GI:317161313 (35); *Streptococcus pneumoniae* AdcA, GI:116516060 (76); *Streptococcus pneumoniae* AdcAII, GI:116515739 (76); *Streptococcus pneumoniae* PiuA, GI:693295764 (77); *Streptococcus pneumoniae* PsaA, GI:116515973 (36); *Streptococcus pyogenes* HtsA GI:114795192 (78); *Streptococcus pyogenes* MtsA, GI:383493478 (33); *Streptococcus suis* TroA, GI:386583456 (79); *Synechocystis* MntC, GI:1653002 (80); *Synechocystis* ZnuA, GI:38492833 (81); *Treponema pallidum* TroA, GI:1777933 (32, 82); *Treponema pallidum* ZnuA, GI:378974662 (82); *Vibrio cholerae* VctP, GI:469674348 (83); *Yersinia pestis* YfeA, GI:1245464 (84); *Yersinia pestis* YfuA GI:913031127 (85); and *Yersinia pestis* ZnuA, GI:25453364 (86). An alignment of these sequences was created using Clustal Omega, and a phylogenetic tree was generated using the neighbor-joining method (87, 88).

***C. trachomatis* growth and metal content determination.** *C. trachomatis* L2 (source ATCC strain 434/Bu) was cultured in McCoy B cells (ATCC CRL-1696) at a multiplicity of infection of 5 until 40 h postinfection, as previously described (89). The *C. trachomatis* cells were isolated from host cell debris after cell lysis using Ultravist gradient-based separation as described previously (90). Whole-cell ICP-MS of the isolated *C. trachomatis* was then performed essentially as described previously (36).

Protein crystallization and structure determination. Purified recombinant, demetallated, tag-free YtgA protein was concentrated to 12 mg/ml using a centrifugal filter unit (MWCO, 10 kDa; Millipore) for crystallization experiments. Equimolar concentration of $FeCl_2$ was added to the protein solution prior to crystallization. The initial hit was obtained from the PACT sparse matrix screen (91). After optimization, diffraction quality Fe-bound YtgA protein crystals were obtained in 22% (wt/vol) polyethylene glycol 6000, 0.2 M $CaCl_2$, 0.01 M $FeCl_2$, and 0.1 M MES (pH 6.0) after 7 days at 18°C using the hanging-drop vapor diffusion method. The Fe(II) supplied in the crystallization solution was likely oxidized to Fe(III) after 3 to 5 days, based on the color change of the solution. Prior to data collection, the crystals were soaked in 25% (vol/vol) glycerol for cryoprotection and then flash-cooled in liquid nitrogen. Diffraction data were collected at cryogenic temperatures from a single crystal at the Australian Synchrotron MX 1 beamline (92) at an X-ray wavelength of 0.954 Å. The data were then processed using XDS (93) and Aimless, CCP4 Suite (94), and the phase information was obtained by molecular replacement by Phaser, Phenix Suite (95) using the crystal structure of pneumococcal PsaA (sequence identity, 21%; PDB 1PSZ) (96) as the search model. The structure model was subsequently created automatically using Phenix.Autobuild (97) and refined iteratively using Phenix.Refine with manual adjustment in COOT (98). Metal ions were modelled based on their peaks in the mF_O-DF_C difference density map, together by consideration of the B factors with their coordination ligands, and chemical plausibility. Structure analyses were performed in PyMOL (Schrödinger, LLC).

Data availability. The YtgA atomic coordinates and structure factors were deposited in the Protein Data Bank under accession number 6NSI.

ACKNOWLEDGMENTS

We acknowledge the use of the Australian Synchrotron MX beamlines, part of ANSTO, and the facilities, and the scientific and technical assistance of the University of Queensland Remote Operation Crystallization and X-ray Diffraction (UQ-ROCX) Facility and Australian Microscopy and Microanalysis Research Facility at the Centre for Microscopy and Microanalysis, The University of Queensland.

This study was supported by National Health and Medical Research Council (NHMRC) Program Grant 1071659 to B.K. and Project Grant 1122582 to C.A.M. and Australian Research Council (ARC) Discovery Project Grant DP170102102 to C.A.M. S.L.N. is an NHMRC Early Career Research Fellow (1142695), B.K. is an NHMRC Principal Research Fellow (1110971) and ARC Laureate Fellow (FL180100109), and C.A.M. is an ARC Future Fellow (FT170100006).

The funders had no role in study design, data collection and interpretation, or the decision to submit the work for publication.

REFERENCES

1. Hentze MW, Muckenthaler MU, Andrews NC. 2004. Balancing acts: molecular control of mammalian iron metabolism. Cell 117:285–297. https://doi.org/10.1016/s0092-8674(04)00343-5.
2. Frey PA, Reed GH. 2012. The ubiquity of iron. ACS Chem Biol 7:1477–1481. https://doi.org/10.1021/cb300323q.
3. Pokorzynski ND, Thompson CC, Carabeo RA. 2017. Ironing out the unconventional mechanisms of iron acquisition and gene regulation in *Chlamydia*. Front Cell Infect Microbiol 7:394. https://doi.org/10.3389/fcimb.2017.00394.
4. Oexle H, Gnaiger E, Weiss G. 1999. Iron-dependent changes in cellular energy metabolism: influence on citric acid cycle and oxidative phosphorylation. Biochim Biophys Acta 1413:99–107. https://doi.org/10.1016/s0005-2728(99)00088-2.
5. Lukianova OA, David SS. 2005. A role for iron-sulfur clusters in DNA repair. Curr Opin Chem Biol 9:145–151. https://doi.org/10.1016/j.cbpa.2005.02.006.
6. Kim HJ, Khalimonchuk O, Smith PM, Winge DR. 2012. Structure, function, and assembly of heme centers in mitochondrial respiratory complexes. Biochim Biophys Acta 1823:1604–1616. https://doi.org/10.1016/j.bbamcr.2012.04.008.

7. West SK. 2004. Trachoma: new assault on an ancient disease. Prog Retin Eye Res 23:381–401. https://doi.org/10.1016/j.preteyeres.2004.04.001.
8. Adderley-Kelly B, Stephens EM. 2005. Chlamydia: a major health threat to adolescents and young adults. ABNF J 16:52–55.
9. Newman L, Rowley J, Vander Hoorn S, Wijesooriya NS, Unemo M, Low N, Stevens G, Gottlieb S, Kiarie J, Temmerman M. 2015. Global estimates of the prevalence and incidence of four curable sexually transmitted infections in 2012 based on systematic review and global reporting. PLoS One 10:e0143304. https://doi.org/10.1371/journal.pone.0143304.
10. Abdelrahman YM, Belland RJ. 2005. The chlamydial developmental cycle. FEMS Microbiol Rev 29:949–959. https://doi.org/10.1016/j.femsre.2005.03.002.
11. Omsland A, Sixt BS, Horn M, Hackstadt T. 2014. Chlamydial metabolism revisited: interspecies metabolic variability and developmental stage-specific physiologic activities. FEMS Microbiol Rev 38:779–801. https://doi.org/10.1111/1574-6976.12059.
12. Stephens RS, Kalman S, Lammel C, Fan J, Marathe R, Aravind L, Mitchell W, Olinger L, Tatusov RL, Zhao Q, Koonin EV, Davis RW. 1998. Genome sequence of an obligate intracellular pathogen of humans: *Chlamydia trachomatis*. Science 282:754–759. https://doi.org/10.1126/science.282.5389.754.
13. Beatty WL, Morrison RP, Byrne GI. 1994. Persistent chlamydiae: from cell culture to a paradigm for chlamydial pathogenesis. Microbiol Rev 58:686–699.
14. Raulston JE. 1997. Response of *Chlamydia trachomatis* serovar E to iron restriction *in vitro* and evidence for iron-regulated chlamydial proteins. Infect Immun 65:4539–4547.
15. Caza M, Kronstad JW. 2013. Shared and distinct mechanisms of iron acquisition by bacterial and fungal pathogens of humans. Front Cell Infect Microbiol 3:80. https://doi.org/10.3389/fcimb.2013.00080.
16. Marx JJ. 2002. Iron and infection: competition between host and microbes for a precious element. Best Pract Res Clin Haematol 15:411–426. https://doi.org/10.1053/beha.2002.0001.
17. Lau CK, Krewulak KD, Vogel HJ. 2016. Bacterial ferrous iron transport: the Feo system. FEMS Microbiol Rev 40:273–298. https://doi.org/10.1093/femsre/fuv049.
18. Perry RD, Mier I, Jr, Fetherston JD. 2007. Roles of the Yfe and Feo transporters of *Yersinia pestis* in iron uptake and intracellular growth. Biometals 20:699–703. https://doi.org/10.1007/s10534-006-9051-x.
19. Miller JD, Sal MS, Schell M, Whittimore JD, Raulston JE. 2009. *Chlamydia trachomatis* YtgA is an iron-binding periplasmic protein induced by iron restriction. Microbiology 155:2884–2894. https://doi.org/10.1099/mic.0.030247-0.
20. Pederick VG, Eijkelkamp BA, Begg SL, Ween MP, McAllister LJ, Paton JC, McDevitt CA. 2015. ZnuA and zinc homeostasis in *Pseudomonas aeruginosa*. Sci Rep 5:13139. https://doi.org/10.1038/srep13139.
21. Plumptre CD, Eijkelkamp BA, Morey JR, Behr F, Couñago RM, Ogunniyi AD, Kobe B, O'Mara ML, Paton JC, McDevitt CA. 2014. AdcA and AdcAII employ distinct zinc acquisition mechanisms and contribute additively to zinc homeostasis in *Streptococcus pneumoniae*. Mol Microbiol 91:834–851. https://doi.org/10.1111/mmi.12504.
22. Petersen TN, Brunak S, von Heijne G, Nielsen H. 2011. SignalP 4.0: discriminating signal peptides from transmembrane regions. Nat Methods 8:785–786. https://doi.org/10.1038/nmeth.1701.
23. Begg SL, Eijkelkamp BA, Luo Z, Couñago RM, Morey JR, Maher MJ, Ong C-LY, McEwan AG, Kobe B, O'Mara ML, Paton JC, McDevitt CA. 2015. Dysregulation of transition metal ion homeostasis is the molecular basis for cadmium toxicity in *Streptococcus pneumoniae*. Nat Commun 6:6418. https://doi.org/10.1038/ncomms7418.
24. Martell AE. 1977. Critical stability constants, vol 3. Plenum Press, New York, NY.
25. Eijkelkamp BA, McDevitt CA, Kitten T. 2015. Manganese uptake and streptococcal virulence. Biometals 28:491–508. https://doi.org/10.1007/s10534-015-9826-z.
26. Couñago RM, McDevitt CA, Ween MP, Kobe B. 2012. Prokaryotic substrate-binding proteins as targets for antimicrobial therapies. Curr Drug Targets 13:1400–1410. https://doi.org/10.2174/138945012803530170.
27. Radka CD, DeLucas LJ, Wilson LS, Lawrenz MB, Perry RD, Aller SG. 2017. Crystal structure of *Yersinia pestis* virulence factor YfeA reveals two polyspecific metal-binding sites. Acta Crystallogr D Struct Biol 73:557–572. https://doi.org/10.1107/S2059798317006349.
28. Radka CD, Labiuk SL, DeLucas LJ, Aller SG. 2019. Structures of the substrate-binding protein YfeA in apo and zinc-reconstituted holo forms. Acta Crystallogr D Struct Biol 75:831–840. https://doi.org/10.1107/S2059798319010866.
29. Trakhanov S, Vyas NK, Luecke H, Kristensen DM, Ma J, Quiocho FA. 2005. Ligand-free and -bound structures of the binding protein (LivJ) of the *Escherichia coli* ABC leucine/isoleucine/valine transport system: trajectory and dynamics of the interdomain rotation and ligand specificity. Biochemistry 44:6597–6608. https://doi.org/10.1021/bi047302o.
30. Felder CB, Graul RC, Lee AY, Merkle HP, Sadee W. 1999. The Venus flytrap of periplasmic binding proteins: an ancient protein module present in multiple drug receptors. AAPS Pharm Sci 1:E2. https://doi.org/10.1208/ps010202.
31. Couñago RM, Ween MP, Begg SL, Bajaj M, Zuegg J, O'Mara ML, Cooper MA, McEwan AG, Paton JC, Kobe B, McDevitt CA. 2014. Imperfect coordination chemistry facilitates metal ion release in the Psa permease. Nat Chem Biol 10:35–41. https://doi.org/10.1038/nchembio.1382.
32. Lee YH, Deka RK, Norgard MV, Radolf JD, Hasemann CA. 1999. *Treponema pallidum* TroA is a periplasmic zinc-binding protein with a helical backbone. Nat Struct Biol 6:628–633. https://doi.org/10.1038/10677.
33. Sun X, Baker HM, Ge R, Sun H, He QY, Baker EN. 2009. Crystal structure and metal binding properties of the lipoprotein MtsA, responsible for iron transport in *Streptococcus pyogenes*. Biochemistry 48:6184–6190. https://doi.org/10.1021/bi900552c.
34. Gribenko A, Mosyak L, Ghosh S, Parris K, Svenson K, Moran J, Chu L, Li S, Liu T, Woods VL, Jr, Jansen KU, Green BA, Anderson AS, Matsuka YV. 2013. Three-dimensional structure and biophysical characterization of *Staphylococcus aureus* cell surface antigen-manganese transporter MntC. J Mol Biol 425:3429–3445. https://doi.org/10.1016/j.jmb.2013.06.033.
35. Abate F, Malito E, Cozzi R, Lo Surdo P, Maione D, Bottomley MJ. 2014. Apo, Zn^{2+}-bound and Mn^{2+}-bound structures reveal ligand-binding properties of SitA from the pathogen *Staphylococcus pseudintermedius*. Biosci Rep 34:e00154. https://doi.org/10.1042/BSR20140088.
36. McDevitt CA, Ogunniyi AD, Valkov E, Lawrence MC, Kobe B, McEwan AG, Paton JC. 2011. A molecular mechanism for bacterial susceptibility to zinc. PLoS Pathog 7:e1002357. https://doi.org/10.1371/journal.ppat.1002357.
37. Yatsunyk LA, Easton JA, Kim LR, Sugarbaker SA, Bennett B, Breece RM, Vorontsov II, Tierney DL, Crowder MW, Rosenzweig AC. 2008. Structure and metal binding properties of ZnuA, a periplasmic zinc transporter from *Escherichia coli*. J Biol Inorg Chem 13:271–288. https://doi.org/10.1007/s00775-007-0320-0.
38. Loisel E, Jacquamet L, Serre L, Bauvois C, Ferrer JL, Vernet T, Di Guilmi AM, Durmort C. 2008. AdcAII, a new pneumococcal Zn-binding protein homologous with ABC transporters: biochemical and structural analysis. J Mol Biol 381:594–606. https://doi.org/10.1016/j.jmb.2008.05.068.
39. Thompson CC, Nicod SS, Malcolm DS, Grieshaber SS, Carabeo RA. 2012. Cleavage of a putative metal permease in *Chlamydia trachomatis* yields an iron-dependent transcriptional repressor. Proc Natl Acad Sci U S A 109:10546–10551. https://doi.org/10.1073/pnas.1201398109.
40. Garmer DR, Gresh N. 1994. A comprehensive energy component analysis of the interaction of hard and soft dications with biological ligands. J Am Chem Soc 116:3556–3567. https://doi.org/10.1021/ja00087a049.
41. Dudev T, Lim C. 2008. Metal binding affinity and selectivity in metalloproteins: insights from computational studies. Annu Rev Biophys 37:97–116. https://doi.org/10.1146/annurev.biophys.37.032807.125811.
42. Ilari A, Alaleona F, Petrarca P, Battistoni A, Chiancone E. 2011. The X-ray structure of the zinc transporter ZnuA from *Salmonella enterica* discloses a unique triad of zinc-coordinating histidines. J Mol Biol 409:630–641. https://doi.org/10.1016/j.jmb.2011.04.036.
43. de Boer M, Gouridis G, Vietrov R, Begg SL, Schuurman-Wolters GK, Husada F, Eleftheriadis N, Poolman B, McDevitt CA, Cordes T. 2019. Conformational and dynamic plasticity in substrate-binding proteins underlies selective transport in ABC importers. Elife 8:e44651.
44. Ba LA, Doering M, Burkholz T, Jacob C. 2009. Metal trafficking: from maintaining the metal homeostasis to future drug design. Metallomics 1:292–311. https://doi.org/10.1039/b904533c.
45. Williams RJ. 1982. Free manganese(II) and iron(II) cations can act as intracellular cell controls. FEBS Lett 140:3–10. https://doi.org/10.1016/0014-5793(82)80508-5.
46. Maret W. 2015. Analyzing free zinc(II) ion concentrations in cell biology with fluorescent chelating molecules. Metallomics 7:202–211. https://doi.org/10.1039/c4mt00230j.
47. van Ooij C, Apodaca G, Engel J. 1997. Characterization of the *Chlamydia trachomatis* vacuole and its interaction with the host endocytic pathway in HeLa cells. Infect Immun 65:758–766.

48. Ouellette SP, Carabeo RA. 2010. A functional slow recycling pathway of transferrin is required for growth of Chlamydia. Front Microbiol 1:112. https://doi.org/10.3389/fmicb.2010.00112.
49. Pan X, Tamilselvam B, Hansen EJ, Daefler S. 2010. Modulation of iron homeostasis in macrophages by bacterial intracellular pathogens. BMC Microbiol 10:64. https://doi.org/10.1186/1471-2180-10-64.
50. Humphrys MS, Creasy T, Sun Y, Shetty AC, Chibucos MC, Drabek EF, Fraser CM, Farooq U, Sengamalay N, Ott S, Shou H, Bavoil PM, Mahurkar A, Myers GS. 2013. Simultaneous transcriptional profiling of bacteria and their host cells. PLoS One 8:e80597. https://doi.org/10.1371/journal.pone.0080597.
51. Scidmore MA, Fischer ER, Hackstadt T. 1996. Sphingolipids and glycoproteins are differentially trafficked to the *Chlamydia trachomatis* inclusion. J Cell Biol 134:363–374. https://doi.org/10.1083/jcb.134.2.363.
52. Al-Younes HM, Rudel T, Brinkmann V, Szczepek AJ, Meyer TF. 2001. Low iron availability modulates the course of *Chlamydia pneumoniae* infection. Cell Microbiol 3:427–437. https://doi.org/10.1046/j.1462-5822.2001.00125.x.
53. Matsumoto A, Bessho H, Uehira K, Suda T. 1991. Morphological studies of the association of mitochondria with chlamydial inclusions and the fusion of chlamydial inclusions. J Electron Microsc (Tokyo) 40:356–363. https://doi.org/10.1093/oxfordjournals.jmicro.a050908.
54. Al-Younes HM, Brinkmann V, Meyer TF. 2004. Interaction of *Chlamydia trachomatis* serovar L2 with the host autophagic pathway. Infect Immun 72:4751–4762. https://doi.org/10.1128/IAI.72.8.4751-4762.2004.
55. Atta M, Nordlund P, Aberg A, Eklund H, Fontecave M. 1992. Substitution of manganese for iron in ribonucleotide reductase from *Escherichia coli*: spectroscopic and crystallographic characterization. J Biol Chem 267:20682–20688.
56. Martin JE, Imlay JA. 2011. The alternative aerobic ribonucleotide reductase of *Escherichia coli*, NrdEF, is a manganese-dependent enzyme that enables cell replication during periods of iron starvation. Mol Microbiol 80:319–334. https://doi.org/10.1111/j.1365-2958.2011.07593.x.
57. Eijkelkamp BA, Morey JR, Ween MP, Ong CL, McEwan AG, Paton JC, McDevitt CA. 2014. Extracellular zinc competitively inhibits manganese uptake and compromises oxidative stress management in *Streptococcus pneumoniae*. PLoS One 9:e89427. https://doi.org/10.1371/journal.pone.0089427.
58. Garcia YM, Barwinska-Sendra A, Tarrant E, Skaar EP, Waldron KJ, Kehl-Fie TE. 2017. A superoxide dismutase capable of functioning with iron or manganese promotes the resistance of *Staphylococcus aureus* to calprotectin and nutritional immunity. PLoS Pathog 13:e1006125. https://doi.org/10.1371/journal.ppat.1006125.
59. Akers JC, HoDac H, Lathrop RH, Tan M. 2011. Identification and functional analysis of CT069 as a novel transcriptional regulator in *Chlamydia*. J Bacteriol 193:6123–6131. https://doi.org/10.1128/JB.05976-11.
60. Posey JE, Hardham JM, Norris SJ, Gherardini FC. 1999. Characterization of a manganese-dependent regulatory protein, TroR, from *Treponema pallidum*. Proc Natl Acad Sci U S A 96:10887–10892. https://doi.org/10.1073/pnas.96.19.10887.
61. Gat O, Mendelson I, Chitlaru T, Ariel N, Altboum Z, Levy H, Weiss S, Grosfeld H, Cohen S, Shafferman A. 2005. The solute-binding component of a putative Mn(II) ABC transporter (MntA) is a novel *Bacillus anthracis* virulence determinant. Mol Microbiol 58:533–551. https://doi.org/10.1111/j.1365-2958.2005.04848.x.
62. Gaballa A, Helmann JD. 1998. Identification of a zinc-specific metalloregulatory protein, Zur, controlling zinc transport operons in *Bacillus subtilis*. J Bacteriol 180:5815–5821.
63. Zawadzka AM, Kim Y, Maltseva N, Nichiporuk R, Fan Y, Joachimiak A, Raymond KN. 2009. Characterization of a *Bacillus subtilis* transporter for petrobactin, an anthrax stealth siderophore. Proc Natl Acad Sci U S A 106:21854–21859. https://doi.org/10.1073/pnas.0904793106.
64. Davis LM, Kakuda T, DiRita VJ. 2009. A *Campylobacter jejuni znuA* orthologue is essential for growth in low-zinc environments and chick colonization. J Bacteriol 191:1631–1640. https://doi.org/10.1128/JB.01394-08.
65. Raulston JE, Miller JD, Davis CH, Schell M, Baldwin A, Ferguson K, Lane H. 2007. Identification of an iron-responsive protein that is antigenic in patients with *Chlamydia trachomatis* genital infections. FEMS Immunol Med Microbiol 51:569–576. https://doi.org/10.1111/j.1574-695X.2007.00336.x.
66. Shi R, Proteau A, Wagner J, Cui Q, Purisima EO, Matte A, Cygler M. 2009. Trapping open and closed forms of FitE: a group III periplasmic binding protein. Proteins 75:598–609. https://doi.org/10.1002/prot.22272.
67. Sabri M, Leveille S, Dozois CM. 2006. A SitABCD homologue from an avian pathogenic *Escherichia coli* strain mediates transport of iron and manganese and resistance to hydrogen peroxide. Microbiology 152:745–758. https://doi.org/10.1099/mic.0.28682-0.
68. Patzer SI, Hantke K. 1998. The ZnuABC high-affinity zinc uptake system and its regulator Zur in *Escherichia coli*. Mol Microbiol 28:1199–1210. https://doi.org/10.1046/j.1365-2958.1998.00883.x.
69. Khambati HK, Moraes TF, Singh J, Shouldice SR, Yu RH, Schryvers AB. 2010. The role of vicinal tyrosine residues in the function of *Haemophilus influenzae* ferric-binding protein A. Biochem J 432:57–64. https://doi.org/10.1042/BJ20101043.
70. Lu D, Boyd B, Lingwood CA. 1997. Identification of the key protein for zinc uptake in *Hemophilus influenzae*. J Biol Chem 272:29033–29038. https://doi.org/10.1074/jbc.272.46.29033.
71. Chen W, Ye D, Wang H, Lin D, Huang J, Sun H, Zhong W. 2013. Binding of oxo-Cu2 clusters to ferric ion-binding protein A from *Neisseria gonorrhoeae*: a structural insight. Metallomics 5:1430–1439. https://doi.org/10.1039/c3mt00091e.
72. Lim KH, Jones CE, Vanden Hoven RN, Edwards JL, Falsetta ML, Apicella MA, Jennings MP, McEwan AG. 2008. Metal binding specificity of the MntABC permease of *Neisseria gonorrhoeae* and its influence on bacterial growth and interaction with cervical epithelial cells. Infect Immun 76:3569–3576. https://doi.org/10.1128/IAI.01725-07.
73. Davies BW, Walker GC. 2007. Disruption of *sitA* compromises *Sinorhizobium meliloti* for manganese uptake required for protection against oxidative stress. J Bacteriol 189:2101–2109. https://doi.org/10.1128/JB.01377-06.
74. Grigg JC, Cooper JD, Cheung J, Heinrichs DE, Murphy ME. 2010. The *Staphylococcus aureus* siderophore receptor HtsA undergoes localized conformational changes to enclose staphyloferrin A in an arginine-rich binding pocket. J Biol Chem 285:11162–11171. https://doi.org/10.1074/jbc.M109.097865.
75. Horsburgh MJ, Wharton SJ, Cox AG, Ingham E, Peacock S, Foster SJ. 2002. MntR modulates expression of the PerR regulon and superoxide resistance in *Staphylococcus aureus* through control of manganese uptake. Mol Microbiol 44:1269–1286. https://doi.org/10.1046/j.1365-2958.2002.02944.x.
76. Bayle L, Chimalapati S, Schoehn G, Brown J, Vernet T, Durmort C. 2011. Zinc uptake by *Streptococcus pneumoniae* depends on both AdcA and AdcAII and is essential for normal bacterial morphology and virulence. Mol Microbiol 82:904–916. https://doi.org/10.1111/j.1365-2958.2011.07862.x.
77. Tai SS, Yu C, Lee JK. 2003. A solute binding protein of *Streptococcus pneumoniae* iron transport. FEMS Microbiol Lett 220:303–308. https://doi.org/10.1016/S0378-1097(03)00135-6.
78. Nygaard TK, Blouin GC, Liu M, Fukumura M, Olson JS, Fabian M, Dooley DM, Lei B. 2006. The mechanism of direct heme transfer from the streptococcal cell surface protein Shp to HtsA of the HtsABC transporter. J Biol Chem 281:20761–20771. https://doi.org/10.1074/jbc.M601832200.
79. Zheng B, Zhang Q, Gao J, Han H, Li M, Zhang J, Qi J, Yan J, Gao GF. 2011. Insight into the interaction of metal ions with TroA from *Streptococcus suis*. PLoS One 6:e19510. https://doi.org/10.1371/journal.pone.0019510.
80. Adir N, Rukhman V, Brumshtein B, Anati R. 2002. Preliminary X-ray crystallographic analysis of a soluble form of MntC, a periplasmic manganese-binding component of an ABC-type Mn transporter from *Synechocystis* sp. PCC 6803. Acta Crystallogr D Biol Crystallogr 58:1476–1478. https://doi.org/10.1107/S0907444902010922.
81. Banerjee S, Wei B, Bhattacharyya-Pakrasi M, Pakrasi HB, Smith TJ. 2003. Structural determinants of metal specificity in the zinc transport protein ZnuA from *Synechocystis* 6803. J Mol Biol 333:1061–1069. https://doi.org/10.1016/j.jmb.2003.09.008.
82. Desrosiers DC, Sun YC, Zaidi AA, Eggers CH, Cox DL, Radolf JD. 2007. The general transition metal (Tro) and Zn^{2+} (Znu) transporters in *Treponema pallidum*: analysis of metal specificities and expression profiles. Mol Microbiol 65:137–152. https://doi.org/10.1111/j.1365-2958.2007.05771.x.
83. Liu X, Du Q, Wang Z, Liu S, Li N, Chen Y, Zhu C, Zhu D, Wei T, Huang Y, Xu S, Gu L. 2012. Crystal structure of periplasmic catecholate-siderophore binding protein VctP from *Vibrio cholerae* at 1.7 Å resolution. FEBS Lett 586:1240–1244. https://doi.org/10.1016/j.febslet.2012.03.043.
84. Bearden SW, Staggs TM, Perry RD. 1998. An ABC transporter system of *Yersinia pestis* allows utilization of chelated iron by *Escherichia coli* SAB11. J Bacteriol 180:1135–1147.
85. Gong S, Bearden SW, Geoffroy VA, Fetherston JD, Perry RD. 2001. Characterization of the *Yersinia pestis* Yfu ABC inorganic iron transport

system. Infect Immun 69:2829–2837. https://doi.org/10.1128/IAI.67.5.2829-2837.2001.
86. Bobrov AG, Kirillina O, Fetherston JD, Miller MC, Burlison JA, Perry RD. 2014. The *Yersinia pestis* siderophore, yersiniabactin, and the ZnuABC system both contribute to zinc acquisition and the development of lethal septicaemic plague in mice. Mol Microbiol 93:759–775. https://doi.org/10.1111/mmi.12693.
87. Larkin MA, Blackshields G, Brown NP, Chenna R, McGettigan PA, McWilliam H, Valentin F, Wallace IM, Wilm A, Lopez R, Thompson JD, Gibson TJ, Higgins DG. 2007. Clustal W and Clustal X version 2.0. Bioinformatics 23:2947–2948. https://doi.org/10.1093/bioinformatics/btm404.
88. Sievers F, Wilm A, Dineen D, Gibson TJ, Karplus K, Li W, Lopez R, McWilliam H, Remmert M, Soding J, Thompson JD, Higgins DG. 2011. Fast, scalable generation of high-quality protein multiple sequence alignments using Clustal Omega. Mol Syst Biol 7:539. https://doi.org/10.1038/msb.2011.75.
89. Huston WM, Theodoropoulos C, Mathews SA, Timms P. 2008. *Chlamydia trachomatis* responds to heat shock, penicillin induced persistence, and IFN-γ persistence by altering levels of the extracytoplasmic stress response protease HtrA. BMC Microbiol 8:190. https://doi.org/10.1186/1471-2180-8-190.
90. Cunningham K, Stansfield SH, Patel P, Menon S, Kienzle V, Allan JA, Huston WM. 2013. The IL-6 response to *Chlamydia* from primary reproductive epithelial cells is highly variable and may be involved in differential susceptibility to the immunopathological consequences of chlamydial infection. BMC Immunol 15:50. https://doi.org/10.1186/1471-2172-14-50.
91. Newman J, Egan D, Walter TS, Meged R, Berry I, Ben Jelloul M, Sussman JL, Stuart DI, Perrakis A. 2005. Towards rationalization of crystallization screening for small- to medium-sized academic laboratories: the PACT/JCSG+ strategy. Acta Crystallogr D Biol Crystallogr 61:1426–1431. https://doi.org/10.1107/S0907444905024984.
92. Cowieson NP, Aragao D, Clift M, Ericsson DJ, Gee C, Harrop SJ, Mudie N, Panjikar S, Price JR, Riboldi-Tunnicliffe A, Williamson R, Caradoc-Davies T. 2015. MX1: a bending-magnet crystallography beamline serving both chemical and macromolecular crystallography communities at the Australian Synchrotron. J Synchrotron Radiat 22:187–190. https://doi.org/10.1107/S1600577514021717.
93. Kabsch W. 2010. XDS. Acta Crystallogr D Biol Crystallogr 66:125–132. https://doi.org/10.1107/S0907444909047337.
94. CCP4. 1994. The CCP4 suite: programs for protein crystallography. Acta Crystallogr D Biol Crystallogr 50:760–763. https://doi.org/10.1107/S0907444994003112.
95. McCoy AJ. 2007. Solving structures of protein complexes by molecular replacement with Phaser. Acta Crystallogr D Biol Crystallogr 63:32–41. https://doi.org/10.1107/S0907444906045975.
96. Lawrence MC, Pilling PA, Epa VC, Berry AM, Ogunniyi AD, Paton JC. 1998. The crystal structure of pneumococcal surface antigen PsaA reveals a metal-binding site and a novel structure for a putative ABC-type binding protein. Structure 6:1553–1561. https://doi.org/10.1016/S0969-2126(98)00153-1.
97. Terwilliger TC, Grosse-Kunstleve RW, Afonine PV, Moriarty NW, Zwart PH, Hung LW, Read RJ, Adams PD. 2008. Iterative model building, structure refinement and density modification with the PHENIX AutoBuild wizard. Acta Crystallogr D Biol Crystallogr 64:61–69. https://doi.org/10.1107/S090744490705024X.
98. Emsley P, Lohkamp B, Scott WG, Cowtan K. 2010. Features and development of Coot. Acta Crystallogr D Biol Crystallogr 66:486–501. https://doi.org/10.1107/S0907444910007493.